1 **Molecular dynamics simulations of noble gases in liquid water: Solvation structure, self-**

2 **diffusion, and kinetic isotope effect**

3

4 Ian C. Bourg[1,*], Garrison Sposito[1]

5

6 [1] Geochemistry Department, Earth Sciences Division, Lawrence Berkeley National Laboratory,

7 Berkeley, CA 94720, USA

8

9

10

11 Both authors contributed equally to research design, data analysis and manuscript writing. The

12 lead author carried out the molecular dynamics simulations.

13

14 Classification: Physical Sciences; Geophysics.

15

16

17 *Author to whom correspondence should be addressed (ibourg@nature.berkeley.edu)

18

19

20   **Abstract**

21

22   Despite their great importance in low-temperature geochemistry, self-diffusion coefficients of

23   noble gas isotopes in liquid water (D) have been measured only for the major isotopes of helium,

24   neon, krypton and xenon. Data on the self-diffusion coefficients of minor noble gas isotopes are

25   essentially non-existent and so typically are estimated by a kinetic theory model in which D

26   varies as the inverse square root of the isotopic mass (m): $D \propto m^{-0.5}$. To examine the validity of

27   the kinetic theory model, we performed molecular dynamics (MD) simulations of the diffusion

28   of noble gases in ambient liquid water with an accurate set of noble gas-water interaction

29   potentials. Our simulation results agree with available experimental data on the solvation

30   structure and self-diffusion coefficients of the major noble gas isotopes in liquid water and reveal

31   for the first time that the isotopic mass-dependence of all noble gas self-diffusion coefficients has

32   the power-law form $D \propto m^{-\beta}$ with $0 < \beta < 0.2$. Thus our results call into serious question the

33   widespread assumption that the 'square root' model can be applied to estimate the kinetic

34   fractionation of noble gas isotopes caused by diffusion in ambient liquid water.

Introduction

35   **Introduction**

36   Dissolved noble gases have proven to be important geochemical indicators of transport

37   processes and paleoclimate in hydrogeological basins (1-7), lacustrine sediments (8-10),

38   aquitards (11-13), engineered clay barriers (14) and the oceans (15). Brennwald et al. (10) used

39   Ne, Ar, Kr and Xe concentrations and ^{20}Ne/^{22}Ne and ^{36}Ar/^{40}Ar isotopic ratios to estimate rates of

40   methane release from anoxic lake sediments. Rübel et al. (12) used ^{4}He concentrations and

41   ^{40}Ar/^{36}Ar isotopic ratios to evaluate the relative importance of advective and diffusive transport

42   in a clay-rich geological formation proposed to become host to a Swiss high-level radioactive

43   waste repository. Stute et al. (1) used Ne, Ar, Kr and Xe concentrations in a Brazilian aquifer to

44   reconstruct continental temperatures during the last 30,000 years. In the paleotemperature

45   reconstruction method of Stute et al. (1), noble gas concentrations in aquifer water were assumed

46   to result from three successive steps: equilibrium dissolution of noble gases at the phreatic

47   surface at the time of groundwater recharge, uptake of excess noble gas through complete

48   dissolution of trapped atmospheric air near the water table, and diffusion-controlled release of a

49   fraction of the excess noble gas (1, 3). For each noble gas other than Ne, the mass fraction

50   released during the third step (1-f_{NG}) is related to the mass fraction of neon released during the

51   third step (1-f_{Ne}) by the well-known Rayleigh fractionation formula (if D_{NG} is the self-diffusion

52   coefficient of a noble gas in water):

53    $$f_{NG} = f_{Ne}^{D_{NG}/D_{Ne}} \qquad\qquad [1]$$

54   Pore water concentrations of the four noble gases Ne, Ar, Kr and Xe then allow the calculation

55   of the four unknown parameter-values: ground temperature and atmospheric pressure at the time

56   and location of groundwater recharge, total amount of dissolved 'excess air', and f_{Ne} (1, 3).

57   Paleotemperatures calculated in this way are most sensitive to Xe concentrations, because the

58   temperature-dependence of noble gas solubility increases with atomic mass (3).

59   Despite the importance of noble gas diffusion coefficients in low-temperature geochemistry,

60   remarkably few measurements of these critical parameters have been reported. Jähne et al. (16)

61   measured self-diffusion coefficients of four noble gases in liquid water at 298 K (Table 1).

62   Pulsed field gradient nuclear magnetic resonance (PFG NMR) studies (17, 18) confirmed the

63   result of Jähne et al. (16) for Ne diffusion, but yielded a significantly larger Xe self-diffusion

64   coefficient (18). No other experimental data on noble gas diffusion in liquid water appear to have

65   been published during the last twenty years. Data on the self-diffusion coefficients of minor

66   noble gas isotopes are even more scarce: they consist of a single measurement of the ratio of the

67   self-diffusion coefficients of ^{3}He and ^{4}He: $D(^{3}\text{He})/D(^{4}\text{He}) = 1.15 \pm 0.03$ (16).

68   With this extreme paucity of experimental data, most geochemical studies of noble gas

69   solutes have relied upon the He, Ne, Kr and Xe diffusion coefficients measured by Jähne et al.

70   (16) together with Ar diffusion coefficients estimated by extrapolation of the results of Jähne et

71   al. (16) (1, 3-6, 8-13, 15, 19). Self-diffusion coefficients of minor noble gas isotopes in liquid

72   water for which no data exist then have routinely been estimated using the kinetic-theory model

73   $D \propto 1/\mu^{0.5}$ [μ is the solvent-solute reduced mass, $\mu = mm_0/(m + m_0)$, if m and m_0 are solute and

74   solvent molecular masses (7)] or, more commonly, the relation $D \propto 1/m^{0.5}$, which is obtained

75   from the kinetic-theory model under the assumption that the hydrogen-bonded water network

76   behaves as an 'effective particle' of infinitely large mass ($m_0 \gg m$) (4, 6, 9, 10, 19). Use of the

77   relation $D \propto 1/m^{0.5}$ in conjunction with measured $^{20}\text{Ne}/^{22}\text{Ne}$ or $^{36}\text{Ar}/^{40}\text{Ar}$ solute isotopic ratios in

78   porous media has led to a widespread dismissal of diffusion in pore water as a significant

4

79   contributor to noble gas transport (4, 6, 10, 19) and, in particular, to strong dismissal (4, 19) of

80   the paleotemperature reconstruction method developed by Stute et al. (1).

81   Very recently Richter et al. (20) discovered somewhat unexpectedly that the self-diffusion

82   coefficients of ionic solutes in liquid water do not follow the 'square-root' model in their

83   dependence on isotopic mass. They provided the first precise measurements of the kinetic

84   fractionation of Mg, Li, and Cl isotopes by diffusion in liquid water and showed that a more

85   general inverse power-law relation, $D \propto m^{-\beta}$, was applicable, with $\beta_{Mg} \sim 0$, $\beta_{Li} = 0.0148 \pm 0.0017$

86   and $\beta_{Cl} = 0.026 \pm 0.014$. Our subsequent molecular dynamics (MD) simulations of the self-

87   diffusion of these ions (21) fully corroborated the small experimental β-values and provided

88   insight based on hydration shell dynamics as to why β differed among the three ions.

89   The very low solubility of noble gases in ambient water currently prevents the use of the

90   experimental method of Richter et al. (20) to measure the mass-dependence of their self-

91   diffusion coefficients (F. M. Richter, personal communication, 2006). The self-diffusion

92   coefficients of noble gas isotopes in liquid water can be calculated, however, by MD simulation.

93   The accuracy of simulations performed for this purpose is limited mainly by the quality of the

94   water-water and noble gas-water intermolecular potentials used. Previous molecular simulations

95   of noble gas solutes in ambient water (22-29) have incorporated noble gas-water potentials

96   calculated either from somewhat outdated noble gas-noble gas interaction data (30) or with

97   approximate (Lorentz-Berthelot) combining rules. Noble gas-water potentials used in these

98   studies were tested only by comparing model predictions with experimental data on the enthalpy

99   and Gibbs energy of hydration. Gibbs energies of noble gas solvation in ambient water were

100   predicted with about 4 kJ mol^{-1} inaccuracy; however, the Gibbs energies of solvation of Ne and

101 Xe differ by only 4.3 kJ mol^{-1} (28). The simulated noble gas self-diffusion coefficients (29) in

102 fact overestimated most experimental data (Table 1).

103 In the present study, MD simulations of noble gas solutes in liquid water were carried out

104 with a new set of noble gas-water potentials calculated with noble gas-noble gas interaction data

105 (31, 32) that are more recent than those of Hirschfelder et al. (30) and with combining rules that

106 are more accurate than the Lorentz-Berthelot rules (33). Our results for the major noble gas

107 isotopes (^{4}He, ^{20}Ne, ^{40}Ar, ^{84}Kr, ^{132}Xe) corroborate available data on their solvation structure (34,

108 35) and self-diffusion coefficients in ambient water (16, 17). Simulations following the

109 methodology of Bourg and Sposito (21) also were performed to determine the isotopic mass-

110 dependence of noble gas self-diffusion coefficients.

111

112 **Solvation structure**

113 The solvation structure near ^{4}He, ^{20}Ne, ^{40}Ar, ^{84}Kr and ^{132}Xe in ambient liquid water as revealed by

114 radial distribution functions is summarized in Figure 1 [radial distribution functions for O and H

115 atoms near noble gas solutes, $g_{NGO}(r)$ and $g_{NGH}(r)$] and Table 2 [location of the first maximum

116 (r_{max}) and minimum (r_{min}) of each $g_{NGO}(r)$ function, and average number of water molecules in the

117 first solvation shell (N_{shell})]. The slightly shorter first-shell peak distance in $g_{NGH}(r)$ as compared

118 to $g_{NGO}(r)$ indicates that first-shell water molecules are preferentially oriented in a "straddling"

119 configuration, such that one of the apices of the water tetrahedron points away from the noble

120 gas atom (36, 37) (Figure 2). This preferred configuration, however, does not require the

121 existence of a static clathrate cage: it exists even for small hydrophobic solutes (H, He, Ne) that

122 diffuse much more rapidly than nearby water molecules and have a 'floppy' solvation shell (38).

123 Radial distribution functions for the smallest noble gas atoms, He and Ne, (Figure 1) are similar

124   to those obtained by Kirchner et al. (38) by *ab initio* MD simulation of a solvated uncharged H

125   atom. The evident absence of solvation structure beyond the first shell is consistent with previous

126   MD simulation studies (23, 25).

127   No experimental data appear to be available concerning the solvation structure around noble

128   gases in ambient liquid water. Bowron et al. (35) used extended X-ray absorption fine-structure

129   (EXAFS) spectroscopy to determine the radial distribution function of O atoms around Kr in

130   water at 20 bar and 277 to 348 K. If the results of Bowron et al. (35) are extrapolated to ambient

131   pressure, based on the lack of pressure-dependence of Kr solvation structure in water between 20

132   to 700 bar (39, 40), they are in good agreement with our MD simulation results (data not shown).

133   Broadbent and Neilson (34) calculated the total distribution function of argon $[G_{Ar}(r)]$ in D_2O at

134   298 K and ~240 bar from isotopic-difference neutron diffraction data on natural Ar ([Nat]Ar) and

135   [36]Ar aqueous solutions. The total distribution function is related to the partial radial distribution

136   functions by:

137 $$G_{Ar}(r) = A\big[g_{NGO}(r) - 1\big] + B\big[g_{NGH}(r) - 1\big] + C\big[g_{ArAr}(r) - 1\big] \qquad [2]$$

138   where the weighting coefficients have the values $A = 1.247$, $B = 2.869$ and $C \approx 0$ at 240 bar (34).

139   Our MD simulation of G_{Ar} based on the partial radial distribution functions is also consistent

140   with the experimental G_{Ar} (data not shown).

141

142   **Self-diffusion coefficients**

143 Experimental and simulation results on the self-diffusion coefficients of major noble gas isotopes

144 in water at 298 K are shown in Table 1 and Figure 3. The self-diffusion coefficients predicted in

145 the present study are consistent with the experimental data of Jähne et al. (16). Notably, our Xe

146 simulation results support the experimental results of Jähne et al. (16), not those of Weingärtner

147   et al. (18). Our Ar simulation results also are consistent with D_{Ar} values estimated by

148   extrapolation of the He, Ne, Kr and Xe diffusion data of Jähne et al. (16) [$D_{Ar} = 2.66 \times 10^{-9}$ m^2 s^{-1}

149   at 298 K (4)].

150

151   **Kinetic fractionation by diffusion in liquid water**

152   The mass dependencies of the self-diffusion coefficients of noble gas isotopes as obtained by

153   MD simulation were analyzed by plotting average log D values obtained during four 2 ns

154   'blocks' of each 8 ns simulation vs. log m. Linear regression of the data shows that the isotopic

155   mass-dependence of noble gas self-diffusion coefficients has the generic power-law form:

156    $$D \propto m^{-\beta} \qquad [3]$$

157   with $\beta > 0$, as proposed originally for ionic solutes by Richter et al. (20) (Linear regression of

158   simulation results as log D vs. log μ yielded a poorer fit than equation 3 for He, Ne, Ar and Xe).

159   The linear regression parameters obtained with equation 3 (Table 3) indicate that $\beta < 0.2$, in

160   stunning contradiction with the kinetic theory model $D \propto 1/m^{0.5}$ (4, 6, 9, 10, 19). For 'Brownian'

161   particles (i.e., solutes that are much larger and heavier than the solvent molecules), the well-

162   known Stokes-Einstein relation predicts that the self-diffusion coefficient should be independent

163   of isotopic mass (i.e., $\beta = 0$ in equation 3). The decrease in β-values in the order He $\geq$ Ne > Ar $\geq$

164   Xe that we observed suggests that the larger noble gas solutes indeed behave in a more

165   'Brownian' manner than do the smaller noble gas solutes. If the solute radius r (Å) is estimated

166   as r_{max} for g_{NGO} (Table 2) minus half of r_{max} for the O-O radial distribution function in pure water

167   (1.4 Å), then our β-values are well described by the power-law relation $\beta = B (1/r)^{\gamma}$ with $B = 0.55$

168   ± 0.17 and $\gamma = 2.49 \pm 0.45$ ($R^2 = 0.98$).

169

170   **Conclusions**

171   A new set of noble-gas water interaction parameters, derived with improved combining rules

172   and noble gas-noble gas interaction parameters, allowed successful prediction of all available

173   experimental data on the solvation structure and self-diffusion coefficients of major noble gas

174   isotopes in ambient liquid water. In particular, our simulation results corroborate the self-

175   diffusion coefficients of major noble gas isotopes measured by Jähne et al. (16) that are widely

176   used in geochemical studies (1, 3-6, 8-13, 15, 19). Our MD simulations carried out with a broad

177   range of solute isotopic masses revealed that noble gas self-diffusion coefficients in water follow

178   an inverse power-law mass-dependence, $D \propto m^{-\beta}$, with $0 < \beta < 0.2$. Thus, the commonly invoked

179   'square root' model of noble gas isotope fractionation by diffusion in liquid water (4, 6, 9, 10,

180   19) overestimates the strength of the mass-dependence of noble gas self-diffusion coefficients.

181

182   **Simulation methods**

183   Molecular dynamics simulations (8 ns interval, preceded by 202 ps of equilibration at 298 K)

184   were carried out with the program MOLDY 3.6 (41) for one noble gas atom and 550 water

185   molecules in a periodically replicated, cubic cell (microcanonical ensemble, 0.997 kg dm^{-3}

186   density) with the methodology of Bourg and Sposito (21). Molecular trajectories were calculated

187   by solving the Newton-Euler equations (with a 1 fs time step) with a form of the Beeman

188   algorithm, the most accurate of all "Verlet-equivalent" algorithms (41). Long-range interactions

189   were treated by Ewald summation with parameters chosen to yield an Ewald sum accuracy of

190   99.99%. Total energy drift during each 8 ns simulation was about 0.002 %. Liquid water was

191   described with the extended simple point charge (SPC/E) model of Berendsen et al. (42). Despite

192   its simplicity [fixed O-H bond lengths (1 Å), H-O-H angle (109.47°) and atomic charges (q_O = -

193   0.8476 e and $q_H = 0.4238$ e)] the SPC/E model predicts the self-diffusion coefficient of water at

194   298 K to within 4 ± 17 % (43), the static dielectric constant of water at 324.2 and 523 K (at 1 kg

195   dm^{-3} density) to within 2 ± 20 and 4 ± 8 % (44), and the X-ray scattering intensities of liquid

196   water at 298 and 350 K to within 1.8 % (45).

197   On the SPC/E model, short-range non-Coulombic interactions (ϕ_{ij}, kJ mol^{-1}) between water O

198   atoms are described with the Lennard-Jones (LJ) 6-12 model:

199
$$\phi_{ij}\left(r_{ij}\right) = 4 \in_{ij} \left[\left(\frac{\sigma_{ij}}{r_{ij}}\right)^6 - \left(\frac{\sigma_{ij}}{r_{ij}}\right)^{12} \right] \qquad [3]$$

200   where r_{ij} (Å) is the interatomic distance and $2^{1/6}\sigma_{ij}$ and $\in_{ij}$ are the location (Å) and depth of the

201   potential well (J mol^{-1}). The LJ 6-12 model, with noble gas σ_{ii} and $\in_{ii}$ parameters compiled by

202   Aziz (31), accurately describes interactions between noble gas atoms in the region of the

203   potential well (32). In the present study, σ_{ij} and $\in_{ij}$ parameters for the interaction between noble

204   gases and water O atoms were calculated from noble gas and SPC/E water σ_{ii} and $\in_{ii}$ parameters

205   with the combining rules of Kong (33):

206
$$\in_{ij} \sigma_{ij}^6 = \sqrt{\in_{ii} \sigma_{ii}^6 \cdot \in_{jj} \sigma_{jj}^6} \qquad [4a]$$

207
$$\in_{ij} \sigma_{ij}^{12} = \left[\frac{\left(\in_{ii} \sigma_{ii}^{12}\right)^{1/13} + \left(\in_{jj} \sigma_{jj}^{12}\right)^{1/13}}{2} \right]^{13} \qquad [4b]$$

208   Equations 4a,b, combined with the kinetic theory of gases, predict self-diffusion coefficients in

209   binary mixtures of noble gases with less than 2 % inaccuracy in a broad temperature range (300

210   to 1400 K), except for Ar-Kr mixtures (33). The same diffusion data, however, are poorly

211   predicted if σ_{ij} and $\in_{ij}$ are calculated with the Lorentz-Berthelot rules (46). The Lennard-Jones

212   parameters used in the present study are compiled in Table 4.

213   Simulations were carried out with ^{4}He, ^{20}Ne, ^{40}Ar, ^{84}Kr and ^{132}Xe isotopes to test the quality

214   of the noble gas-water interaction potentials in Table 4, and with a range of hypothetical isotopes

215   of He, Ne, Ar and Xe (m = 4-132 Da) to determine the isotopic mass dependence of solute self-

216   diffusion coefficients. Previous studies have used MD simulation with a broad range of solute

217   mass to infer solute isotopic effects, mainly in Lennard-Jones or hard-sphere fluids (47-49) but

218   also in liquid water (21, 50, 51). Radial distribution functions of O and H atoms near noble gas

219   (NG) solutes and noble gas velocity autocorrelation functions ($<\mathbf{v}(0)\cdot\mathbf{v}(t)>$) were calculated with

220   standard methods (41, 52). The average number of oxygen atoms in the first solvation shell of

221   each noble gas (N_{shell}) was calculated by integrating the function $4\pi r^2 g_{NGO}(r)$ to its first minimum

222   (r_{min}). Solute self-diffusion coefficients were calculated with the well-known Green-Kubo

223   relation (52):

224    $$D = \frac{1}{3}\lim_{\tau\to\infty}\int_0^\tau \langle\mathbf{v}(0)\cdot\mathbf{v}(t)\rangle dt \qquad [5]$$

225   The 'infinite limit' in equation 5 was approximated accurately by taking the average of D-values

226   obtained for τ = 2.4 to 2.5 ps.

227

228   **Acknowledgments**

References

1. Stute M, Forster M, Frischkorn H, Serejo A, Clark JF, Schlosser P, Broecker WS, Bonani G (1995) *Science* 269:379-383

2. Castro MC, Goblet P, Ledoux E, Violette S, de Marsily G (1998) *Water Resour Res* 34:2467-2483.

3. Aeschbach-Hertig W, Peeters F, Beyerle U, Kipfer R (1999) *Water Resour Res* 35:2779-2792.

4. Peeters F, Beyerle U, Aeschbach-Hertig W, Holocher J, Brennwald MS, Kipfer R (2002) *Geochim Cosmochim Acta* 67:587-600.

5. Price RM, Top Z, Happell JD, Swart PK (2003) *Water Resour Res* 39:1267.

6. Zhou Z, Ballentine CJ, Kipfer R, Schoell M, Thibodeaux S (2005) *Geochim Cosmochim Acta* 69:5413-5428.

7. LaBolle EM, Fogg G.E, Eweis JB (2006) *Water Resour Res* 42:W07202.

8. Poreda RJ, Hunt AG, Lyons WB, Welch KA (2004) *Aquat Geochem* 10:353-371.

9. Strassmann KM, Brennwald MS, Peeters F, Kipfer R (2005) *Geochim Cosmochim Acta* 69: 1665-1674.

10. Brennwald MP, Kipfer R, Imboden DM (2005) *Earth Planet Sci Lett* 235:31-44.

11. Osenbrück K, Lippmann J, Sonntag J (1998) *Geochim Cosmochim Acta* 62:3041-3045.

12. Rübel AP, Sonntag C, Lippmann J, Pearson FJ, Gautschi A (2002) *Geochim Cosmochim Acta* 66:1311-1321.

13. Hendry MJ, Kotzer TG, Solomon DK (2005) *Geochim Cosmochim Acta* 69:475-483.

14. Higashihara T, Shibuya H, Sato S, Kozaki T (2005) *Eng Geol* 81:365-370.

15. Rodehacke CB, Hellmer HH, Huhn O, Beckmann A (2007) *Ocean Dyn* 57:1-11.

16. Jähne B, Heinz G, Dietrich W (1987) *J Geophys Res* 92:10767-10776.

17. Holz M, Haselmeier R, Mazitov RK, Weingärtner H (1994) *J Am Chem Soc* 116:801-802.

18. Weingärtner H, Haselmeier R, Holz M (1992) *Chem Phys Lett* 195:596-601.

19. Klump S, Tomonaga Y, Kienzler P, Kinzelbach W, Baumann T, Imboden DM, Kipfer R (2007) *Geochim Cosmochim Acta* 71:1385-1397.

20. Richter FM, Mendybaev RA, Christensen JN, Hutcheon ID, Williams RW, Sturchio NC, Beloso AD, Jr (2006) *Geochim Cosmochim Acta* 70:277-289.

21. Bourg IC, Sposito G (2007) *Geochim Cosmochim Acta*, in press.

22. Swope WC, Andersen HC (1984) *J Phys Chem* 88:6548-6556.

23. Straatsma TP, Berendsen HJC, Postma JPM (1986) *J Chem Phys* 85:6720-6727.

24. Tanaka H, Nakanishi K (1991) *J Chem Phys* 95:3719-3727.

25. Guillot B, Guissani Y, Bratos S (1991) *J Chem Phys* 95:3643-3648.

26. Lazaridis T, Paulaitis ME (1994) *J Phys Chem* 98, 635-642.

27. Lau EY, Gerig JT (1995) *J Chem Phys* 103:3341-3349.

28. Arthur JW, Haymet ADJ (1998) *J Chem Phys* 109:7991-8002.

29. Ohmori T, Kimura Y (2005) in *Proceedings of the 14th International Conference on the Properties of Water and Steam*, eds Nakahara M et al (Maruzen Co, Ltd), pp 160-165.

30. Hirschfelder JO, Curtiss CF, Bird RB (1954) *Molecular Theory of Gases and Liquids* (Wiley, New York).

31. Aziz RA (1984) in *Inert Gases: Potentials, Dynamics and Energy Transfer in Doped Crystals*, ed Klein M (Springer, New York), pp 5-86.

32. Tang KT, Toennies JP (1986) *Z Phys D* 1:91-101.

33. Kong CL (1973) *J Chem Phys* 59:2464-2467.

34. Broadbent RD, Neilson GW (1994) *J Chem Phys* 100:7543-7547.

35. Bowron DT, Filipponi A, Lobban C, Finney JL (1998) *Chem Phys Lett* 293:33-37.

36. Geiger A, Rahman A, Stillinger FH (1979) *J Chem Phys* 70:263-276.

37. Rapaport DC, Scheraga HA (1982) *J Phys Chem* 86:873-880.

38. Kirchner B, Stubbs J, Marx D (2002) *Phys Rev Lett* 89:215901.

39. Filipponi A, Bowron DT, Lobban C, Finney JL (1997) *Phys Rev Lett* 79:1293-1296.

40. Bowron DT, Weigel R, Filipponi A, Roberts MA, Finney JL (2001) *Mol Phys* 99:761-765.

41. Refson K (2000) *Comput Phys Commun* 126:310-329.

42. Berendsen HJC, Grigera JR, Straatsma TP (1987) *J Phys Chem* 91:6269-6271.

43. Smith DE, Dang LX (1994) *J Chem Phys* 100:3757-3766.

44. Wasserman E, Wood B, Brodholt J (1995) *Geochim Cosmochim Acta* 70:277-289.

45. Hura G, Russo D, Gleaser RM, Head-Gordon T, Krack M, Parrinello M (2003) *Phys Chem Chem Phys* 5:1981-1991.

46. Hogervorst W (1971) *Physica* 51:77-89.

47. Alder BJ, Alley WE, Dymond JH (1974) *J Chem Phys* 61:1415-1420.

48. Nuevo MJ, Morales JJ, Heyes DM (1995) *Phys Rev E* 51:2026-2032.

49. Willeke M (2003) *Mol Phys* 101:1123-1130.

50. Wilson MA, Pohorille A, Pratt LR (1985) *J Chem Phys* 83:5832-5836.

51. Møller KB, Rey R, Masia M, Hynes JT (2005) *J Chem Phys* 122:114508.

52. Allen MP, Tildesley DJ (1987) *Computer Simulation of Liquids* (Clarendon Press, Oxford).

Table 1. Self-diffusion coefficients (10^{-9} m^2 s^{-1}) of noble gases in ambient liquid water.

Noble gas	Experimental (16)	Experimental (17, 18)	MD simulation (29)	MD simulation (this study)
He	7.22 ± 0.36		10.0 ± 0.9	7.85 ± 0.54
Ne	4.16 ± 0.21	4.18 ± 0.20	4.9 ± 0.2	4.78 ± 0.37
Ar			2.4 ± 0.1	2.57 ± 0.15
Kr	1.84 ± 0.09		2.1 ± 0.1	1.97 ± 0.13
Xe	1.47 ± 0.07	1.90 ± 0.09[a]	1.6 ± 0.1	1.57 ± 0.11

[a] confidence interval calculated with the assumption that NMR data for Ne and Xe diffusion have similar coefficients of variation.

Table 2. Location of the first maximum and minimum of $g_{NGO}(r)$ and first-shell coordination number of O atoms around noble gas solutes in ambient liquid water. Confidence intervals on r_{max} and r_{min} values are ± 0.05 Å.

Noble gas	r_{max} (Å)	r_{min} (Å)	N_{shell}
He	3.0	4.7	14.0 ± 0.4
Ne	3.1	4.9	15.7 ± 0.4
Ar	3.5	5.2	18.8 ± 0.5
Kr	3.7	5.4	21.2 ± 0.5
Xe	3.9	5.6	22.4 ± 0.5

Table 3. Parameters of the linear regression equation $\log(D) = A - \beta \cdot \log(m)$ calculated with 16 paired D,m values for each noble gas solute.

Solute	A	β	R^2
He	1.00 ± 0.04	0.171 ± 0.028	0.91
Ne	0.87 ± 0.03	0.150 ± 0.018	0.95
Ar	0.52 ± 0.04	0.078 ± 0.024	0.75
Xe	0.33 ± 0.03	0.059 ± 0.023	0.65

Table 4. Lennard-Jones 6-12 potential parameters.

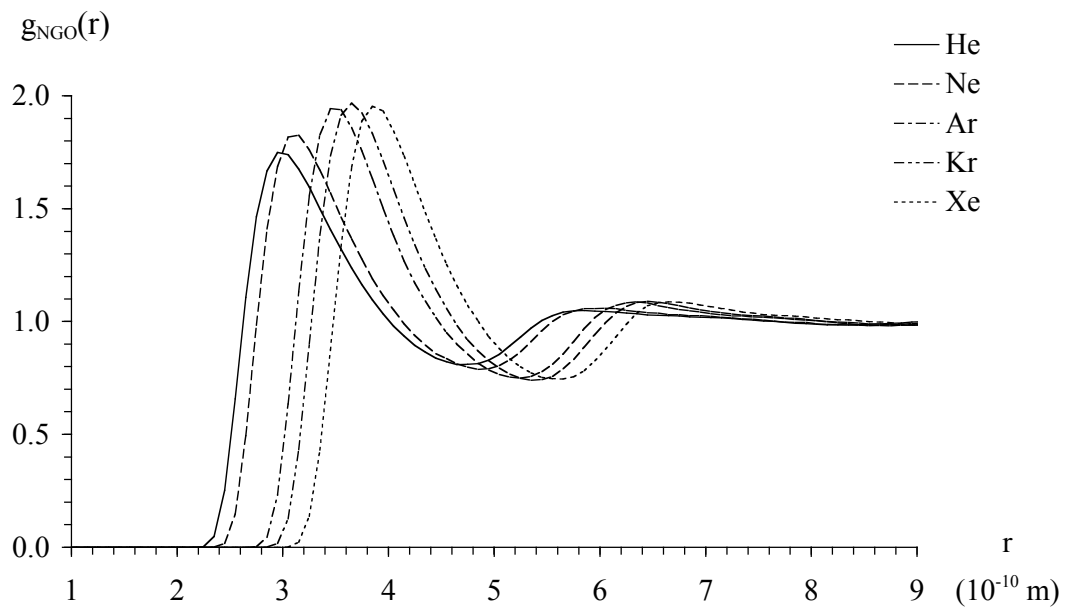| Atom pair	σ (Å)	$\in$ (kJ mol^{-1})
Noble gas-water interaction		
He-O	2.9730	0.20500
Ne-O	2.9758	0.45416
Ar-O	3.2645	0.86608
Kr-O	3.3948	0.98380
Xe-O	3.5874	1.07990
Water-water interaction (42)		
O-O	3.1656	0.65017

List of Figures

Fig. 1. Radial distribution functions of (a) O atoms and (b) H atoms near noble gases in liquid water at 298 K.

Fig. 2. Snapshot of a ^{40}Ar atom (in green) and water molecules located in its first solvation shell (i.e., at Ar-O distances < 5.2 Å). Highlighted water molecules in the upper and lower parts of the figure illustrate the two possible 'straddling' configurations, with either a lone pair of electrons (upper part of the figure) or an H atom (lower part of the figure) pointing away from the solute.

Fig. 3. Experimental and simulated self-diffusion coefficients of noble gases in liquid water at 298 K, plotted as a function of solute radius.
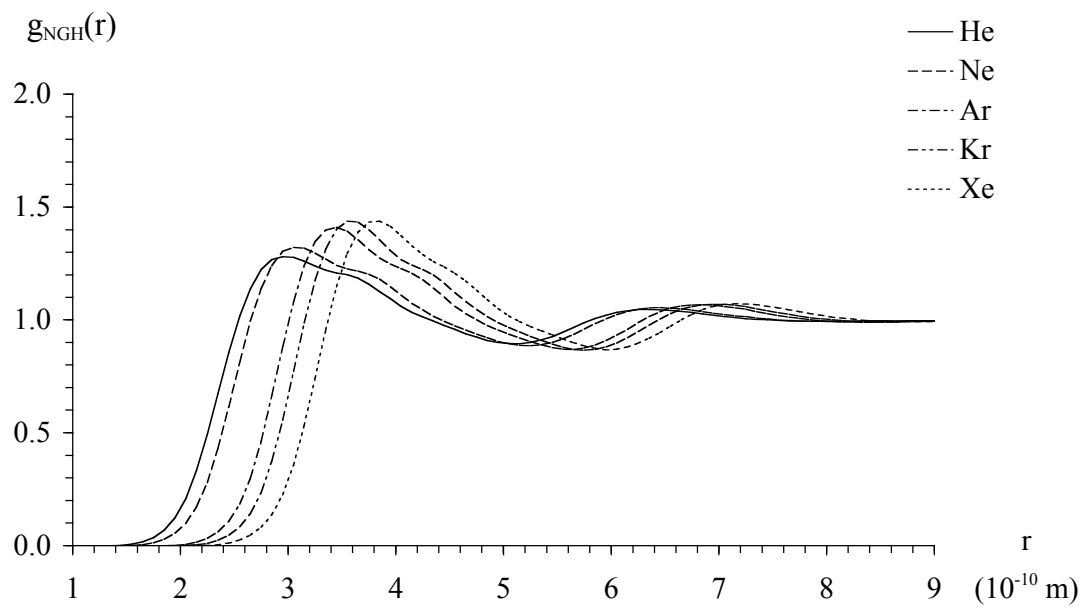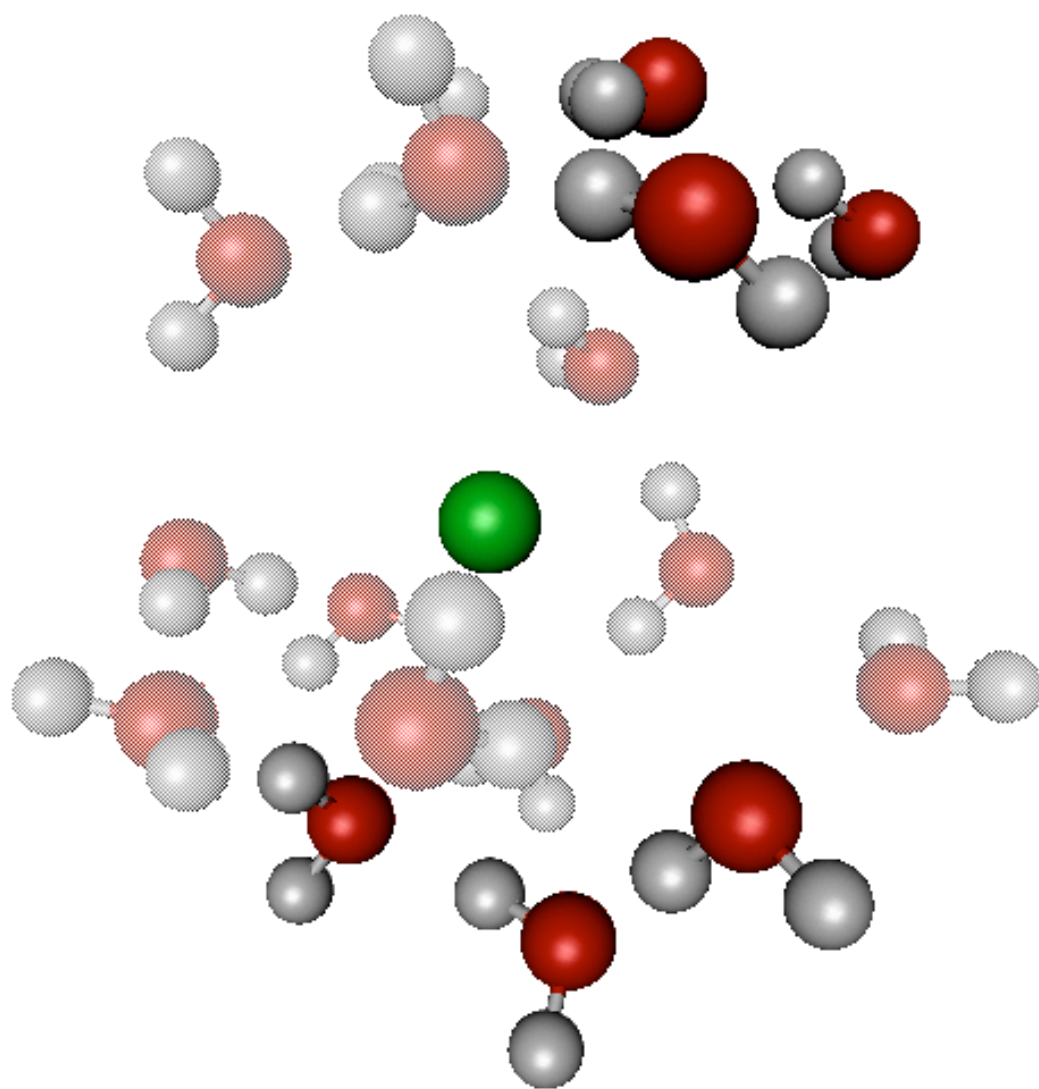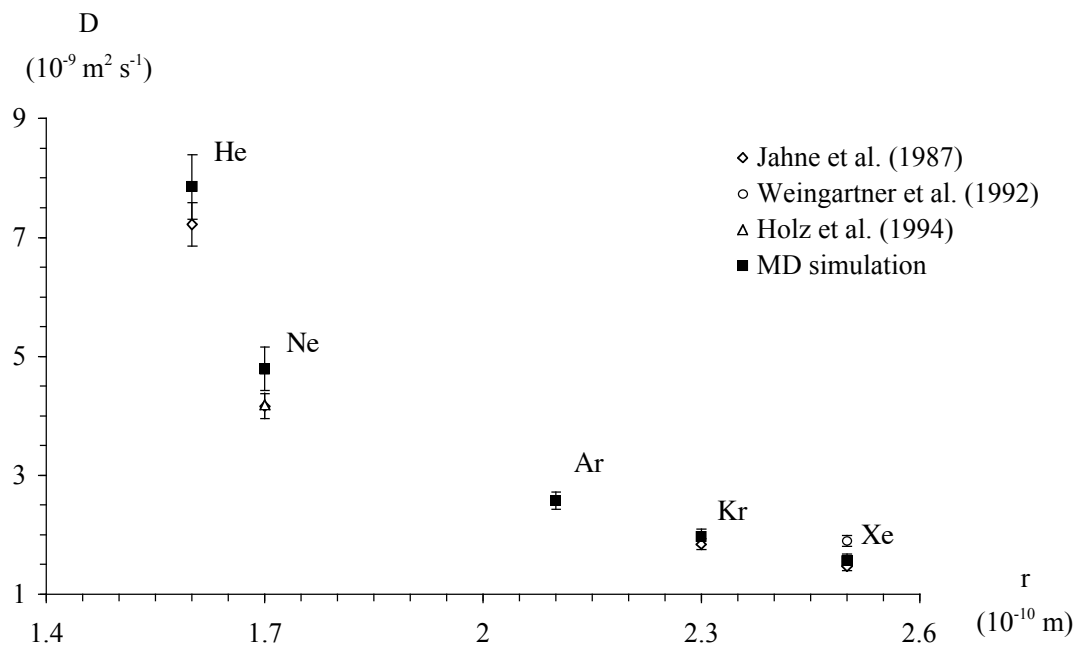
a)

b)

Figure 1.

Figure 2.

D
$(10^{-9}\ m^2\ s^{-1})$

He

◇ Jahne et al. (1987)
○ Weingartner et al. (1992)
△ Holz et al. (1994)
■ MD simulation

Ne

Ar

Kr

Xe

r
$(10^{-10}\ m)$

9

7

5

3

1

1.4   1.7   2   2.3   2.6

Figure 3.